

Combinatorial approach to identify electronically cloaked hollow nanoparticles

Wenqing Shen,¹ Tao Tian,¹ Bolin Liao,² and Mona Zebarjadi^{1,3}

¹*Department of Mechanical and Aerospace Engineering, Rutgers University, Piscataway, New Jersey 08854, USA*

²*Department of Mechanical Engineering, Massachusetts Institute of Technology, Cambridge, Massachusetts 02139, USA*

³*Institute of Advanced Materials, Devices, and Nanotechnology, Rutgers University, New Brunswick, New Jersey 08901, USA*

(Received 5 May 2014; published 4 August 2014)

The possibility of designing core-shell nanoparticles that are “invisible” to the conduction electrons has been demonstrated recently. A total scattering cross section smaller than 0.01% of the physical cross section was demonstrated by artificially adjusting the parameters of the barrier and the well in a core-shell geometry. In this paper, we aim to extend the developed concept and find realistic material combinations that satisfy the cloaking criteria. We report designs of hollow nanoparticles that could be used to realize the cloaking concept in III–V semiconductor host matrices. Such particles could be used in advanced materials design to enhance and tune the electrical and the thermoelectric properties of a given host matrix. This paper may also contribute to defect engineering by coating defect sites with a proper cloaking layer.

DOI: [10.1103/PhysRevB.90.075301](https://doi.org/10.1103/PhysRevB.90.075301)

PACS number(s): 81.05.Xj, 61.46.Df, 72.80.Ey, 72.20.Pa

I. INTRODUCTION

Modern materials design has enabled us to tune material properties and design materials with unprecedented characteristics that cannot be found in nature. The introduction of metamaterials has paved the way for an entirely new venue in future technologies.

A key advance in metamaterial design is the cloaking concept, i.e., design of objects invisible to a particular range of waves. This concept has been transposed to different fields to produce materials with extreme properties and to design new devices. Electromagnetic or optical cloaking was proved possible by using a transformation-optics method [1,2] and scattering cancellation via homogeneous and isotropic shells [3]. It is shown that acoustical parameters in the cloak should be anisotropic to achieve acoustic cloaking [4,5]. Finally, experiments were done to demonstrate thermal cloaking in a copper plate [6] and thermally conductive sealant [7].

By analogy with these examples, electronic cloaking [8–12] could be used for quantum sensing [10]. Recently, the idea of electronic cloaking has been introduced with the promise of designing advanced semiconductors with extremely high electrical conductivities [9] and enhanced thermoelectric properties [8]. Using two-dimensional (2D) electronic cloaking, new 2D devices have been proposed [13], such as filters, sensors, and switches. This paper is a step towards a practical realization of such materials.

Semiconductor materials are usually doped with a high concentration of external impurity atoms to provide the required level of conduction carrier (electrons/holes) densities for a good electronic performance. The electrical conductivity, σ , of a material is proportional to the product of the charge carrier density and its mobility ($\sigma = ne\mu$). Carrier mobility, μ , characterizes how fast conduction carriers move through a solid-state material. It depends on the interaction potential of the scattering centers with the conduction carriers and therefore could be manipulated by using the freedom of design and engineering the interaction potential of the scattering centers. By cloaking the carrier donating centers, carrier mobility could be significantly improved [14].

Carrier mobility is a key material parameter in determining the performance of semiconductor-based devices such as transistors, light-emitting diodes (LEDs), solar cells, thermoelectric applications, etc. [15–17]. Increased charge carrier mobility for many applications is desired for enabling an increase in the electrical conductivity of semiconductor devices, and it almost always leads to better device performances with other parameters being equal. The approaches of scattering cross-section cancellation [9] and transportation optics [12] were proved to improve carrier mobility.

In the case of semiconductors, the external impurity atoms used for doping act as scattering centers and randomize the motion of conduction carriers, thus limiting their mobility. In our previous study, we demonstrated that it is possible to replace conventional dopants with invisible dopants [8]. In order to realize this goal, we added all the dopants inside spherical nanoparticles and then designed a cloaking cover around the nanoparticles to make them invisible to the conduction electrons. The nanoparticles used, therefore, had core-shell structure. These nanoparticles were artificial, as their band offsets (between core and shell and between shell and host) and effective masses were tuned numerically to satisfy the cloaking conditions; i.e., the scattering cross section was small enough to be considered negligible. For real materials, band offsets and effective masses are set by the nature of the material and might not be consistent with adjusted parameters. Therefore, the designed nanoparticles in the previous work might not correspond to any realistic material. By using artificial nanoparticles, an order of magnitude increase in the electrical conductivity and, consequently, the thermoelectric power factor of GaAs at low temperatures was demonstrated. In addition, it was speculated that the nanoparticles might reduce the thermal conductivity [18], if materials with large acoustic mismatch are used for the core-shell.

The next question is the possibility of designing realistic core-shell nanoparticles with real material properties as the input and investigating their effectiveness for improving the electrical conductivity and enhancing the Seebeck coefficient of a given host matrix, which is the focus of this paper.

The paper is organized in the following manner: A combinatorial search algorithm is proposed to obtain proper material characteristics that may achieve electron cloaking. Then, the results for several host matrices are reported. Finally, a complete optimization is reported for one of the materials combinations.

II. METHODOLOGY

The cross section of scattered waves by a spherically symmetric potential is calculated by the partial wave method [19]. The total cross section of electrons with a specific incident energy is given as [19]

$$\sigma = \frac{4\pi}{k^2} \sum_{l=0}^{\infty} (2l+1) \sin^2 \delta_l, \quad (1)$$

where δ_l is the phase shift of the l th partial wave, and $k = \frac{\sqrt{2m_0 E}}{\hbar}$ is the wave number, where m_0 is the effective mass of the host matrix, and E is the energy of electron [9].

The phase shifts of higher-order partial waves are small and could be neglected if their angular momentum, l , is larger than ka ($l > ka$), where a is the outer radius of the nanoparticle [19]. Thus, a negligible total scattering cross section could be achieved by eliminating the scattering cross section of the first two partial waves and using ka values close to or less than one.

To reduce the number of variables and simplify the search, we use hollow nanoparticles whose core is a vacuum. Today, many different hollow nanoparticles, such as PbTe [20], gold [21], Cu₂O, ZnS, ZnO, and many others, have been fabricated successfully [22], making the choice of hollow nanoparticle possible. In this paper, we only consider such hollow nanoparticles as shown in Fig. 1. In this figure, a and a_c are the radii of the shell and the core, respectively. The

terms m_{core} , m_{shell} , and m_{host} are the effective mass for vacuum, shell, and host material, respectively. $E_{c,\text{host}}$ and $E_{c,\text{shell}}$ are the conduction levels of host and shell, and ΔE_{c1} and ΔE_{c2} are the band offset of the core-shell and the shell-host, respectively. We assume that the bands are aligned according to Anderson's rule.

We used a combinatorial approach to find proper material combinations. For an efficient search, we started from a rough scan, which ignores charge transfer and band bending. For a given host material and targeted hollow nanoparticle, the only relevant parameters that may affect the scattering cross section are electron incident energy (E), core size (a_c), shell size (a), the shell layer's effective mass (m_{shell}), and the band offset between the shell and the host (ΔE_{c2}).

Small nanoparticles correspond to smaller ka values, which correspond to faster decay of high-order partial wave terms in Equation (1). For a small size nanoparticle, there is a better chance of having negligible high-order partial waves. However, a_c and a cannot be too small for practical purposes. We set $a_c = 1$ nm and $a = 2$ – 3 nm for our rough scan. If we do not see a cloaking point for such small particles, the chances of observing cloaking for larger particles would be small, as reflected by the trend of Fig. 2.

For thermoelectric applications, heavily doped semiconductors are used, and the optimum Fermi level (the Fermi level corresponding to the optimum power factor) is known for a given thermoelectric material. For example, the optimum Fermi level for GaAs at room temperature is around 63 meV above the conduction band edge, which is calculated from optimum carrier density [23]. Since only electrons in the Fermi window contribute to the transport, the electron incident energy should be set only to values close to the optimum Fermi level.

Setting all of the parameters as described above, we only need to scan for the two remaining parameters, which are ΔE_{c2} and m_{shell} . It is then feasible to plot the scattering cross section versus these two parameters and set upper and lower bounds for them. Once the ranges are determined, one can look up a materials database and find proper shell materials whose effective masses and band offsets with the host matrix fall in the determined range.

Our criterion for selecting the parameters range is when an electron-nanoparticle scattering cross section $< 1\%$ of the physical cross section (πa^2) is achieved. We refer to this region as the *cloaking region*. After obtaining a proper shell material from the rough search, we further optimize the size and the doping density of the embedded hollow nanoparticles in the given host matrix.

III. RESULTS AND DISCUSSIONS

Figure 2 shows the total electron-nanoparticle scattering cross section at incident energy $E = 150$ meV versus m_{shell} and ΔE_{c2} . The host material is Ga_{0.2}In_{0.8}As; the outer radius of the shell is increased slowly as shown in Figs. 2(a) to 2(d). The bright region in Fig. 2, which corresponds to scattering cross section $< 1\%$ of the physical cross section, is the cloaking region. From these results, we can determine that the value of the proper m_{shell} is generally around 0–0.1 m_0 (m_0 is the mass of electron), and ΔE_{c2} is around -0.2 eV

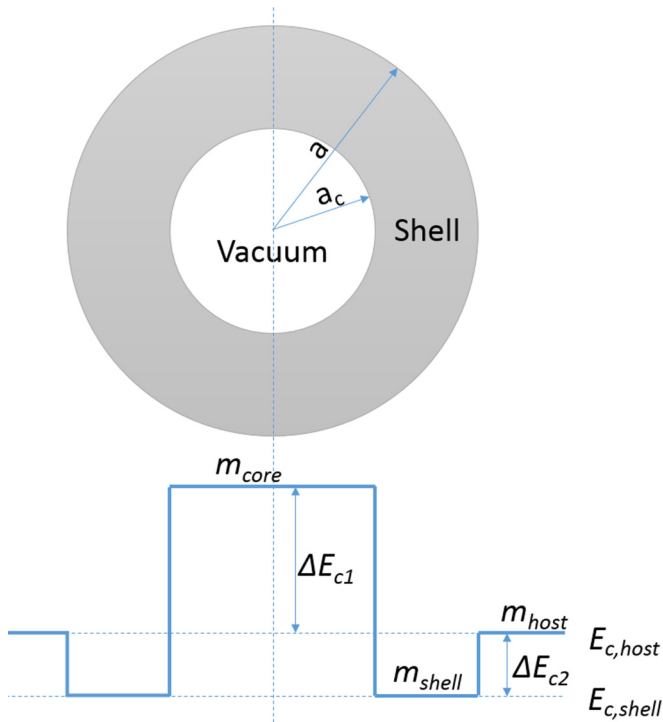


FIG. 1. (Color online) Structure of a hollow nanoparticle.

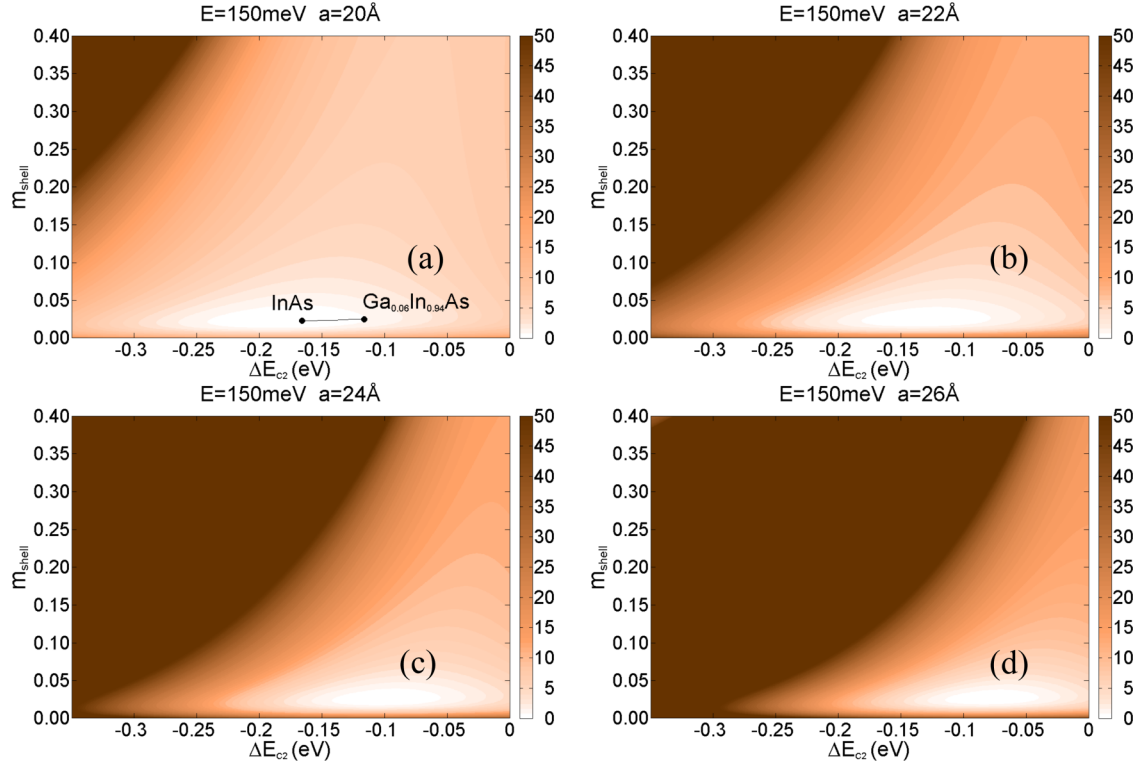


FIG. 2. (Color online) The effect of shell properties on the normalized scattering cross-section (%) contours. The scattering cross section is calculated for $\text{Ga}_{0.2}\text{In}_{0.8}\text{As}$ (as the host matrix) with a fixed electron energy $E = 150$ meV. The size of the vacuum core is also fixed at $a_c = 1$ nm. We then scan the possible effective masses and band offsets for the shell to identify proper shells. (a) $a = 20$ Å, (b) $a = 22$ Å, (c) $a = 24$ Å, (d) $a = 26$ Å.

to 0 eV for $\text{Ga}_{0.2}\text{In}_{0.8}\text{As}$ being the host matrix. We refer to this range of values as the cloaking range of each parameter. The cloaking region becomes smaller and moves towards the coordinate's origin as the nanoparticle size increases. That is, the cloaking range of m_{shell} and ΔE_{c2} shrinks and shifts to smaller values for larger nanoparticles. With a fixed shell thickness, as shown in Fig. 3, the cloaking region also decreases, and the m_{shell} cloaking range shrinks as the electron incident energy increases. However, the ΔE_{c2} cloaking range does not change greatly with increasing E . Note that this is merely our numerical results observation, and we do not have a clear explanation for these trends.

Once this initial scan is performed and the cloaking ranges for each parameter are determined, we can choose proper shell materials for the given host. As an example, for the chosen materials here, $\text{Ga}_{0.2}\text{In}_{0.8}\text{As}$ [Fig. 2(a)], we can see that InAs and alloys of $\text{Ga}_{0.06}\text{In}_{0.94}\text{As}$ fall in the cloaking region. Using InAs as the shell and $\text{Ga}_{0.2}\text{In}_{0.8}\text{As}$ as the host, “cloaking” can be achieved. Furthermore, a slight diffusion of Ga from the host matrix to the shell layer (up to 6%) would not affect the results significantly.

In the next step, we will further optimize the size and the doping density of the selected materials (i.e., InAs/ $\text{Ga}_{0.2}\text{In}_{0.8}\text{As}$).

As shown in Fig. 4, the cloaking range of a and E is decreasing when a_c is increasing. For a small shell thickness, the total scattering cross section increases with increasing E , while for larger thicknesses, the total cross section first decreases and then rises with increasing E ; that is, there is an

antiresonance dip in the scattering cross section. For a smaller a_c , the E cloaking range is larger, creating more choices for the corresponding Fermi level. Also by comparing (a)–(d) in Fig. 4, we find that a similar shell thickness is required for different core sizes. With similar “good” shell thicknesses, the scattering cross-section dip is found at a smaller energy value for a larger core.

We have scanned a large class of materials, including GaAs, InAs, InP, PbTe, Bi_2Te_3 , and their alloys such as $\text{Ga}_x\text{In}_{1-x}\text{As}$, to find realistic material combinations. Results for some of the other host materials are shown in Fig. 5. For Bi_2Te_3 , InAs, GaAs, InP, and PbTe, the optimum Fermi level is about 130 meV [15], 67 meV [23], 63 meV [23], 30 meV [23], and 20 meV [24], respectively, which were calculated from optimum carrier density at 300 K. Points in each graph show some of the possible shell materials identified for that particular host matrix. Among these points, the lattice constant of GaInSb does not match well with GaAs. There still exists great chance to find other proper shells by considering more materials and lowering the temperature, which would increase the range of proper parameters and make it easier to find matched materials.

After finding the proper shell/host combination as described above, we take one of the optimal combinations to calculate the actual scattering cross section, including charge transfer from the doped shell layer to the host. For the first nanoparticle (np1), the radius of the core is 1.5 nm, and the radius of the total nanoparticle is 2.7 nm. For the second nanoparticle (np2), the radius of the core and the shell is 3.5 nm and

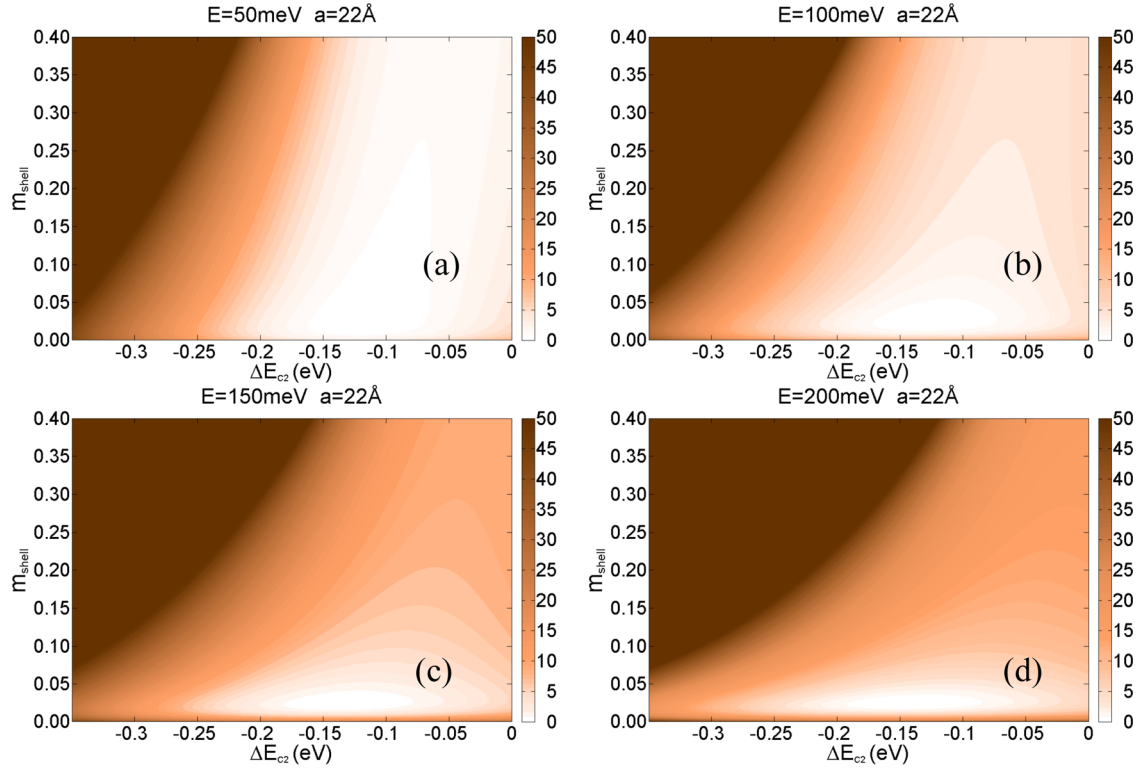


FIG. 3. (Color online) The effect of electron energy on normalized scattering cross section (%) for fixed host material and nanoparticle geometric structure. $\text{Ga}_{0.2}\text{In}_{0.8}\text{As}$ is taken as the host matrix, and the outer radius of the shell is fixed at $a = 22 \text{ \AA}$. (a) $E = 50 \text{ meV}$, (b) $E = 100 \text{ meV}$, (c) $E = 150 \text{ meV}$, (d) $E = 200 \text{ meV}$.

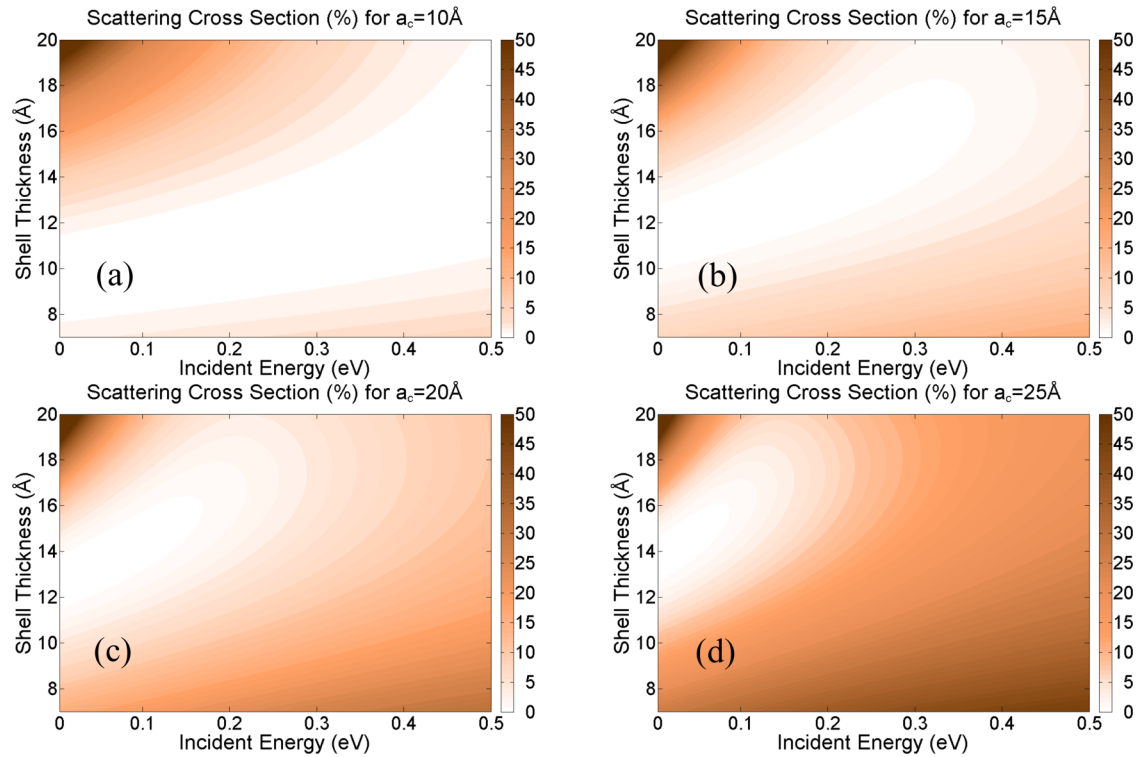


FIG. 4. (Color online) Effect of nanoparticle sizes on the normalized scattering cross section (%) for a specific materials combination: InAs is taken as the shell, and $\text{Ga}_{0.2}\text{In}_{0.8}\text{As}$ as the host matrix. The radii of the cores are set to (a) $a_c = 10 \text{ \AA}$, (b) $a_c = 15 \text{ \AA}$, (c) $a_c = 20 \text{ \AA}$, (d) $a_c = 25 \text{ \AA}$.

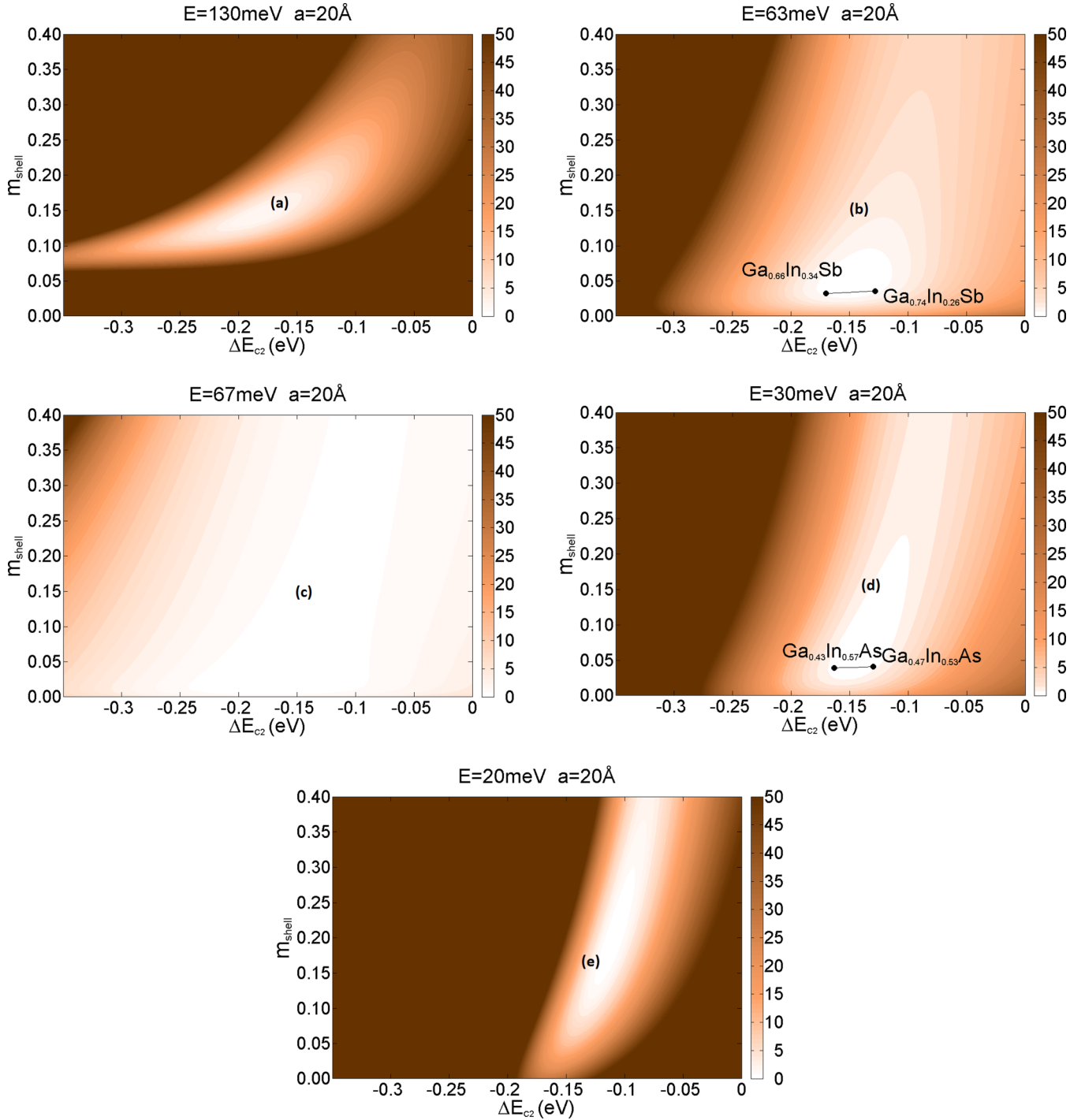


FIG. 5. (Color online) Normalized scattering cross section (%) for (a) Bi_2Te_3 , (b) GaAs, (c) InAs, (d) InP, (e) PbTe. $a = 10 \text{ \AA}$ and $a_c = 20 \text{ \AA}$ are set for these calculations.

5.0 nm respectively. These sizes are obtained from Fig. 4. $\text{Ga}_{0.2}\text{In}_{0.8}\text{As}$ is taken as the host, and InAs is the shell material of the nanoparticle, while the core is vacuum. The material's parameters are reported in the Appendix. For GaInAs, we consider alloy, polar optical phonons, acoustic phonons, and impurity scatterings [25] in addition to nanoparticle scattering, and we use Matthiessen's rule to calculate the total scattering rate. We use linearized transport integrals [26] to calculate the thermoelectric transport coefficients including

the Seebeck coefficient, electrical conductivity, and finally the thermoelectric power factor. Using the parameters reported in the Appendix, we were able to reproduce the electron mobility values reported in the literature for GaInAs (see Appendix). Each nanoparticle is assumed to donate one electron to the host matrix ($Z = 1$), and different densities of nanoparticles produce different doping densities ($1 \times 10^{13} - 2 \times 10^{17} \text{ cm}^{-3}$). The potential profile for np2 is shown in Fig. 6, from which we can see a lower potential both at the core and at the shell

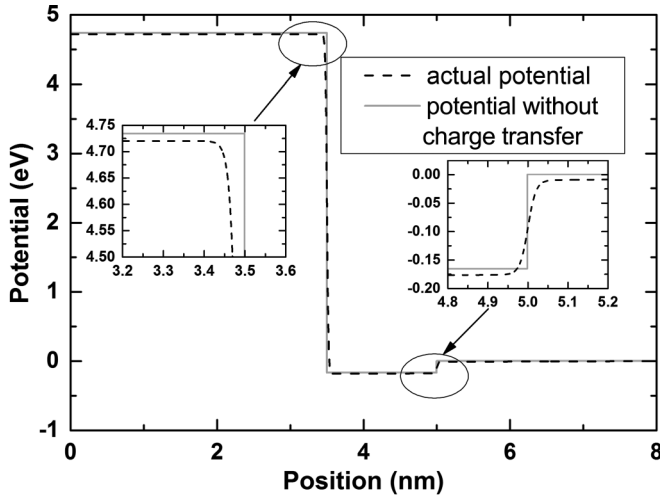


FIG. 6. Potential profile as a function of position in radial direction for np2 after considering carrier. The dashed line labeled “actual potential” shows the actual potential with consideration of charge transfer. The radius of the core is 3.5 nm, and the outer radius of the shell is 5.0 nm. Only one electron is doped per nanoparticle. $\text{Ga}_{0.2}\text{In}_{0.8}\text{As}$ is taken as the host, and InAs as the shell material of the nanoparticle while the core is vacuum.

than that without charge transfer. After considering the charge transfer, “cloaking” can still be achieved, as shown in Fig. 7. The minimal total cross section at the dip is less than 1% of the physical cross section. Both np1 and np2 show a scattering dip, but the corresponding electron energy is very different. All the partial waves contribute to the total cross section, while the phase shifts of higher-order partial waves are relatively small if ka is less than 1, making the summation in Equation (1) converge rapidly [19]. Since np2 has a larger size (a) compared to np1, it requires a smaller electron energy to achieve a similar ka value. Therefore, the corresponding energies and the energy

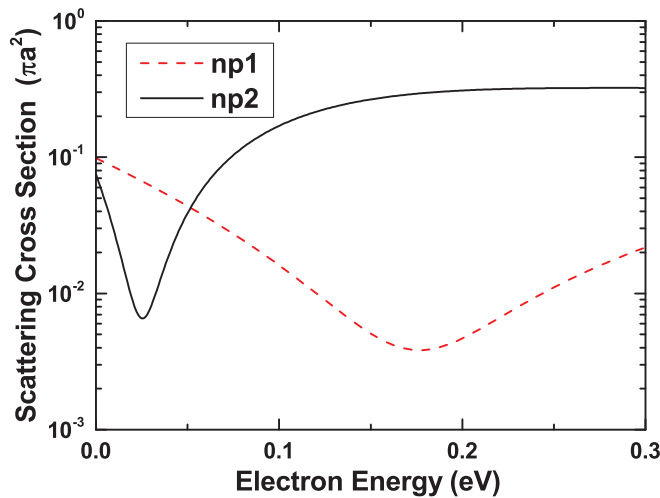


FIG. 7. (Color online) Scattering cross section for np1 and np2 as a function of electron energy. Both the minimum scattering cross sections are less than 1%, illustrating the achievement of invisibility of the nanoparticle.

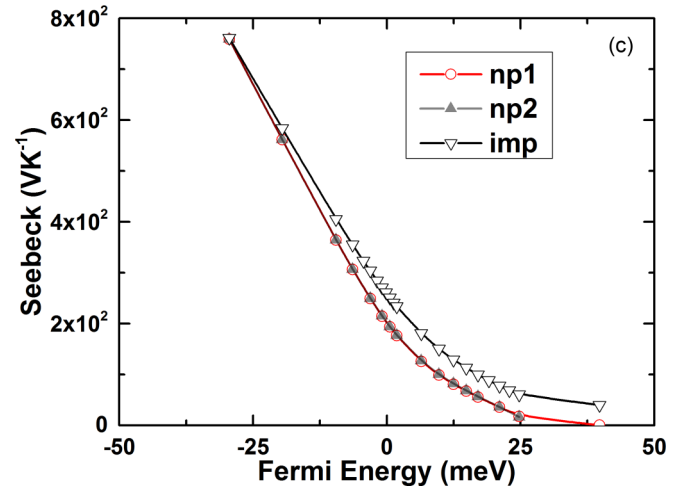
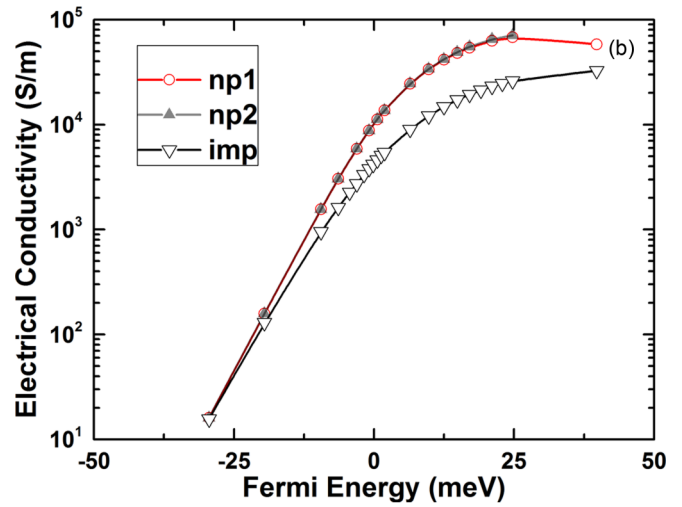
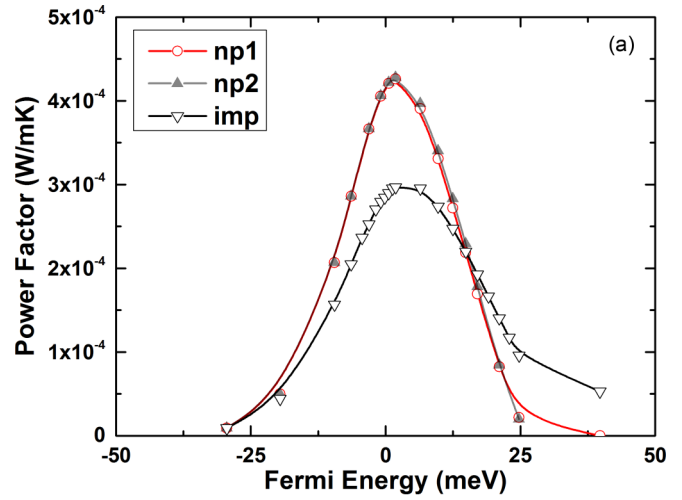


FIG. 8. (Color online) Comparison of the power factor for different samples. The line labeled by “imp” shows the uniform impurity-doped sample.

dip of np2 are shifted to smaller values compared to np1 (see Fig. 7).

Figure 8(a) shows the power factor improvement using a hollow nanoparticle. As can be seen, antiresonance nanoparticles can improve the thermoelectric power factor

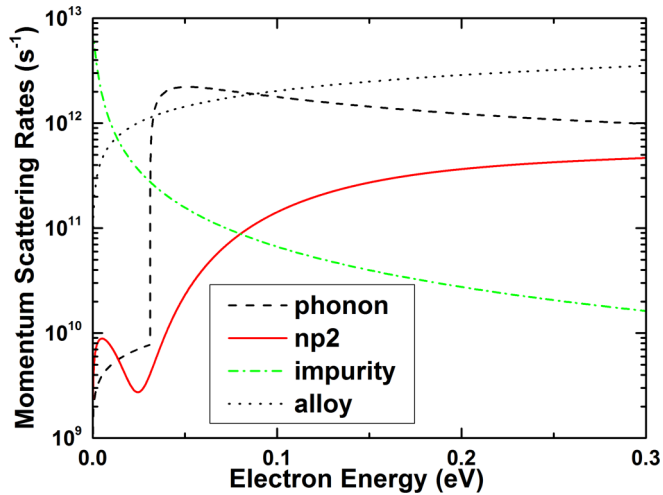


FIG. 9. (Color online) Momentum scattering rates of different kinds for $\text{Ga}_{0.2}\text{In}_{0.8}\text{As}$ at 50 K. “Phonon” refers to the electron scattering by polar optical and acoustic phonons. “Impurity” is calculated at the optimum Fermi level using a traditional ionized impurity-doped sample, and “np2” shows the scattering rate by nanoparticle 2 at the optimum Fermi level. Scattering by alloy in np2 sample is also plotted.

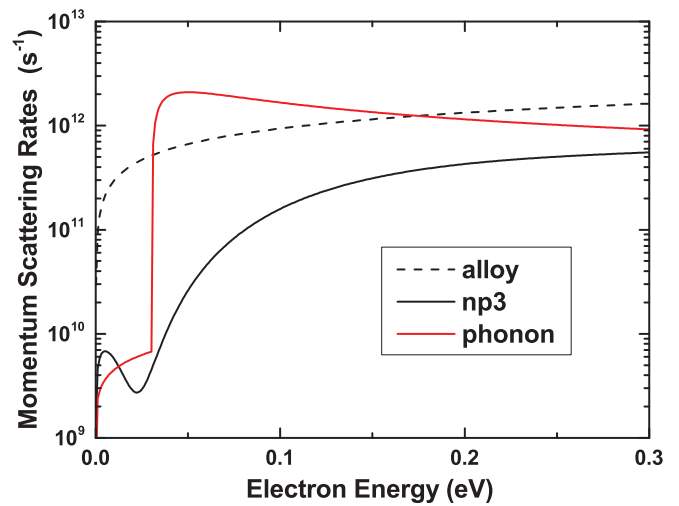


FIG. 11. (Color online) Momentum scattering rates of different kinds for $\text{Ga}_{0.1}\text{In}_{0.9}\text{As}$ at 50 K. “Phonon” refers to the electron scattering by polar optical and acoustic phonons. Black solid line “np3” shows the scattering rate by nanoparticle 3. Red solid line refers to alloy scattering.

significantly. The peaks of the power factor for np1 and np2 have an improvement of 45%, as compared to the host doped with uniform impurity. We can also see from Fig. 8(b) that np1 and np2 show a conductivity that is several times larger than the impurity-doped sample, which is expected since the scattering rates are much lower when conventional dopants are replaced by the designed hollow nanoparticles. The Seebeck coefficient is slightly decreased for the hollow nanoparticle embedded sample [Fig. 8(c)]. An increase is expected in the Seebeck coefficient as a result of introducing sharp features in relaxation times and therefore in the differential conductivity [27]. However, it should be noted that after replacing conventional dopants with the designed hollow nanoparticles, the scattering

is dominated by the background phonon and alloy scattering in the Fermi window and, therefore, the scattering dip does not enhance the Seebeck coefficient. Figure 9 shows important scattering rates versus energy in the host matrix. The alloy scattering rate is the dominant scattering rate in the hollow nanoparticle-doped sample. Thus, the power factor does not vary significantly when the nanoparticle size is changed. The optimum Fermi levels for np1, np2, and the impurity-doped sample are all found at about 5 meV, as shown in Fig. 7(a). The scattering dip is found at around 20 meV for np1 and at around 160 meV for np2; the former is closer to the optimum Fermi level. However, due to the background scatterings, the power factor, mobility, and Seebeck coefficient appear similar for np1 and np2, as shown in Fig. 8.

These results are very encouraging, since they are not nanoparticle parameter sensitive, and therefore the enhancement is observable even if there is randomness to some degree in the nanoparticle sizes.

The main role of the designed nanoparticles is to minimize the doping scattering rates. The hollow nanoparticle doping method shows a significant advantage over that of the uniform doping method. This type of doping is most effective in samples where doping scattering rates are the dominant scattering mechanisms and the other rates are negligible. To demonstrate the importance of background scattering, we performed calculations using $\text{Ga}_{0.1}\text{In}_{0.9}\text{As}$ as the host, and leaving other parameters unchanged. The results show an over 80% improvement of a maximum power factor by substituting the impurity with hollow nanoparticles, as shown in Fig. 10. According to the analysis for $\text{Ga}_{0.2}\text{In}_{0.8}\text{As}$, alloy scattering plays a major role. For $\text{Ga}_{0.1}\text{In}_{0.9}\text{As}$, there is less alloy scattering than for $\text{Ga}_{0.2}\text{In}_{0.8}\text{As}$, emphasizing the importance of the background scattering, which can be seen by comparing Figs. 9 and 11.

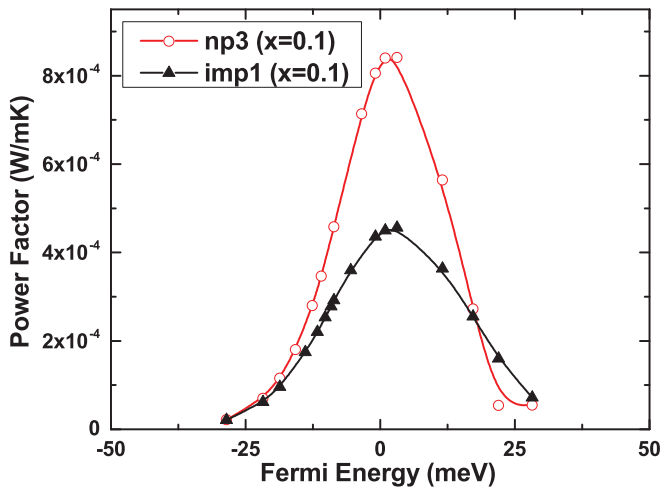


FIG. 10. (Color online) Power factor vs Fermi energy using $\text{Ga}_{0.1}\text{In}_{0.9}\text{As}$ as the host. The np3 has the same core-shell structure as np2. The “imp1” shows the results for a uniform-doped sample.

TABLE I. Property of materials.

Material	Electron effective mass (m_e)	Electron affinity (eV)
InAs [28]	0.023	4.9
Ga _x In _{1-x} As [28]	(0.023+0.037x+0.003x ²)	(4.9-0.83x)
InP [28]	0.08	4.38
GaAs [28]	0.063	4.07
PbTe	0.3 [29]	4.6 [30]
Bi ₂ Te ₃	0.28 [31]	(4.125-4.525) [32]

IV. CONCLUSIONS

From this paper, we can conclude that the concept of an antiresonant nanoparticle renders the enhancement of electrical conductivity and the power factor possible. In this paper, we have identified several possible hollow nanoparticles/host material combinations including InAs/InGaAs and InP/GaInAs. The material of the host matrix and nanoparticle is not limited to those shown in this paper. We introduced a simple combinational search method to identify proper shell/host combinations. There exists a great chance to find other and even much better material combinations. The advantage of antiresonant nanoparticles is much more significant for samples where doping scattering is the dominant scattering mechanism and the other background scatterings are weak. The strategy developed here may be expanded to improve the design of semiconductor materials with better electronic and thermoelectric properties, which can be applied in many different fields.

ACKNOWLEDGMENTS

We would like to acknowledge Prof. G. Chen for useful discussion. W. S. would like to thank Yasmeen Ragi for her help in revising the writing. Work at MIT is supported by S³TEC, an Energy Frontier Research Center funded by the

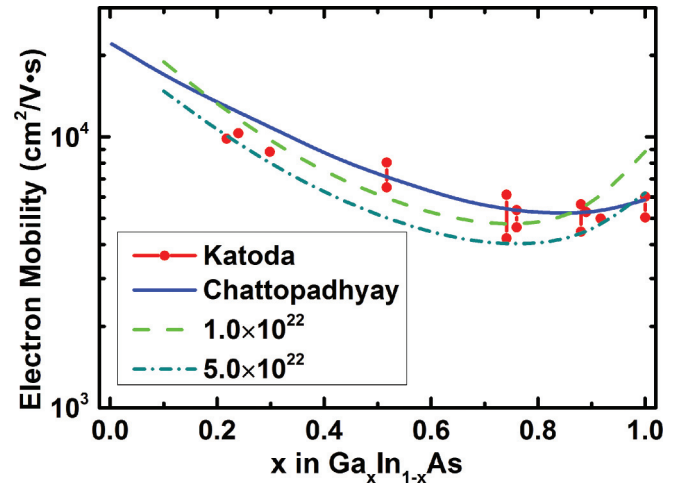


FIG. 12. (Color online) Electron mobility versus x for Ga_xIn_{1-x}As. “Katoda” refers the experiment data with carrier density in the range of 1.0×10^{22} – 5.0×10^{22} m⁻³, “Chattopadhyay” shows the numerical result with carrier density set at 4.0×10^{22} m⁻³, and “ 1.0×10^{22} ” and “ 5.0×10^{22} ” show our calculation results using $n = 1.0 \times 10^{22}$ m⁻³ and $n = 5.0 \times 10^{22}$ m⁻³, respectively. All the data are for room temperature.

U.S. Department of Energy, Office of Basic Energy Sciences, under Award No. DE-FG02-09ER46577.

APPENDIX

The electron effective mass and electron affinity used in this paper are listed in Table I.

To verify that the host property of Ga_xIn_{1-x}As used for calculation is credible, Fig. 12 shows the comparison among our calculation results and data from other groups [33,34]. Our results are consistent with others’ data.

- [1] U. Leonhardt, *Science* **312**, 1777 (2006).
- [2] J. B. Pendry, D. Schurig, and D. R. Smith, *Science* **312**, 1780 (2006).
- [3] A. Alù and N. Engheta, *Phys. Rev. E* **72**, 016623 (2005).
- [4] A. N. Norris, *Proc. R. Soc. A Math. Phys. Eng. Sci.* **464**, 2411 (2008).
- [5] S. A. Cummer, B.-I. Popa, D. Schurig, D. R. Smith, J. Pendry, M. Rahm, and A. Starr, *Phys. Rev. Lett.* **100**, 024301 (2008).
- [6] R. Schittny, M. Kadic, S. Guenneau, and M. Wegener, *Phys. Rev. Lett.* **110**, 195901 (2013).
- [7] T. Han, X. Bai, D. Gao, J. T. L. Thong, B. Li, and C.-W. Qiu, *Phys. Rev. Lett.* **112**, 054302 (2014).
- [8] M. Zebarjadi, B. Liao, K. Esfarjani, M. Dresselhaus, and G. Chen, *Adv. Mater.* **25**, 1577 (2013).
- [9] B. Liao, M. Zebarjadi, K. Esfarjani, and G. Chen, *Phys. Rev. Lett.* **109**, 126806 (2012).
- [10] R. Fleury and A. Alù, *Phys. Rev. B* **87**, 201106 (2013).
- [11] R. Fleury and A. Alù, *Phys. Rev. B* **87**, 045423 (2013).
- [12] M. G. Silveirinha and N. Engheta, *Phys. Rev. B* **86**, 161104 (2012).
- [13] B. Liao, M. Zebarjadi, K. Esfarjani, and G. Chen, *Phys. Rev. B* **88**, 155432 (2013).
- [14] M. Zebarjadi, G. Joshi, G. Zhu, B. Yu, A. Minnich, Y. Lan, X. Wang, M. Dresselhaus, Z. Ren, and G. Chen, *Nano Lett.* **11**, 2225 (2011).
- [15] G. J. Snyder and E. S. Toberer, *Nat. Mater.* **7**, 105 (2008).
- [16] A. Bolognesi, A. Di Carlo, and P. Lugli, *Appl. Phys. Lett.* **81**, 4646 (2002).
- [17] M.-A. Muth, W. Mitchell, S. Tierney, T. A. Lada, X. Xue, H. Richter, M. Carrasco-Orozco, and M. Thelakkat, *Nanotechnology* **24**, 484001 (2013).
- [18] W. Kim, J. Zide, A. Gossard, D. Klenov, S. Stemmer, A. Shakouri, and A. Majumdar, *Phys. Rev. Lett.* **96**, 045901 (2006).
- [19] I. L. Schiff, *Quantum Mechanics* (McGraw-Hill, New York, 1949).
- [20] G. Zou, Z. Liu, D. Wang, C. Jiang, and Y. Qian, *Eur. J. Inorg. Chem.* **2004**, 4521 (2004).
- [21] X. Pang, L. Zhao, W. Han, X. Xin, and Z. Lin, *Nat. Nanotechnol.* **8**, 426 (2013).

- [22] H. J. Fan, U. Gösele, and M. Zacharias, *Small* **3**, 1660 (2007).
- [23] N. Mingo, *Appl. Phys. Lett.* **84**, 2652 (2004).
- [24] T. C. Harman, D. L. Spears, and M. P. Walsh, *J. Electron. Mater.* **28**, L1 (1999).
- [25] M. Lundstrom, *Fundamentals of Carrier Transport*, 2nd ed. (Cambridge University Press, Cambridge, 2000).
- [26] H. J. Goldsmid, *Introduction to Thermoelectricity (Springer Series in Materials Science)* (Springer-Verlag, Berlin, Heidelberg, 2010), Chap. 3.
- [27] G. D. Mahan and J. O. Sofo, *Proc. Natl. Acad. Sci.* **93**, 7436 (1996).
- [28] Semiconductors on NSM, <http://www.ioffe.rssi.ru/SVA/NSM/Semicond/> (2013).
- [29] H. Lyden, *Phys. Rev.* **135**, A514 (1964).
- [30] W. Spicer and G. Lapeyre, *Phys. Rev.* **139**, A565 (1965).
- [31] C. Jeong, R. Kim, M. Luisier, S. Datta, and M. Lundstrom, *J. Appl. Phys.* **107**, 023707 (2010).
- [32] J. Nagao, E. Hatta, and K. Mukasa, in *Fifteenth Int. Conf. Thermoelectr. Proc. ICT '96* (IEEE, Pasadena, CA, 1996), pp. 404–407.
- [33] T. Katoda, F. Osaka, and T. Sugano, *Jpn. J. Appl. Phys.* **13**, 561 (1974).
- [34] D. Chattopadhyay, S. K. Sutradhar, and B. R. Nag, *J. Phys. C Solid State Phys.* **14**, 891 (1981).